Fast and Slow Responses of the Tropical Pacific to Radiative Forcing in Northern High Latitudes

HUNG-YI TSENG,[a] YEN-TING HWANG,[a] SHANG-PING XIE,[b] YU-HENG TSENG,[c] SARAH M. KANG,[d]
MATTHEW T. LUONGO,[b] AND IAN EISENMAN[b]

[a] *Department of Atmospheric Sciences, National Taiwan University, Taipei, Taiwan*
[b] *Scripps Institution of Oceanography, University of California, San Diego, La Jolla, California*
[c] *Institute of Oceanography, National Taiwan University, Taipei, Taiwan*
[d] *School of Urban and Environmental Engineering, Ulsan National Institute of Science and Technology, Ulsan, South Korea*

ABSTRACT: This study investigates the transient evolution of tropical Pacific sea surface temperature (SST) responses to a constant northern high-latitude solar heating in fully coupled CESM 1.2. The study identifies two stages through multiple ensemble runs. 1) In the first 3 years, a hemispherically asymmetric pattern emerges, caused by air–sea interactions associated with the anomalous cross-equatorial Hadley cell. The northern tropics experience warming that is blocked north of the equator by the intertropical convergence zone. The southeast Pacific cooling reaches the equatorial region and is amplified by the equatorial Ekman divergence. 2) Within a decade, the equatorial cooling is replaced by warming in the eastern equatorial basin. The anomalous warming that appears faster than the time scales of the oceanic ventilation is attributed to anomalous meridional heat convergence and weakening of the northern subtropical cell. Our findings highlight the influence of ocean dynamics on the temporal and spatial evolution of tropical SST response to hemispherically asymmetric heating. The initial cooling caused by Ekman divergence delays the arrival of slow warming, while initial wind and temperature anomalies set the stage for the weakening of the subtropical cell. The results have important implications for understanding the evolution of tropical SST patterns in observational records and future climate change simulations, as they show strong interhemispheric temperature asymmetry in the extratropics.

KEYWORDS: Atmosphere-ocean interaction; General circulation models; Pacific Ocean; Sea surface temperature; Teleconnections

1. Introduction

Energy perturbations from high latitudes can penetrate deeply into the tropical Pacific regions, imposing significant influences on the sea surface temperature (SST) pattern, and subsequently influencing both local and global climates. Changes in the interhemispheric meridional SST gradient are reported in various modeling experiments that impose a range of extratropical forcings, such as sea ice or ice sheet perturbations (Chiang and Bitz 2005), reductions in the Atlantic meridional overturning circulation (Zhang and Delworth 2005), increases of anthropogenic sulfate aerosol emissions (Yoshimori and Broccoli 2008), anomalous Southern Ocean heat uptake (Hwang et al. 2017), and idealized thermal heat fluxes (Broccoli et al. 2006; Hwang et al. 2021; Kang et al. 2008). In addition, imposing anomalous freshwater in the North Atlantic leads to a collapse of the Atlantic meridional overturning circulation and triggers an El Niño event (Dong and Sutton 2002). The so-called El Niño–Southern Oscillation (ENSO)–like SST response pattern, with the anomalous SST peaking at the eastern equatorial Pacific region, has been demonstrated in the semi-equilibrium state in several simulations with various mid–high-latitude variations, such as the loss of Arctic sea

ice (Deser et al. 2015; England et al. 2020; Tomas et al. 2016), high-latitude insolation reductions (Kang et al. 2020), and extratropical cloud bias corrections (Burls et al. 2017). In short, the signals originating outside the tropics largely modulate the structure of tropical Pacific SST.

Several mechanisms have been proposed to interpret the tropical SST responses to extratropical forcing. On one hand, the thermodynamical interactions between the atmosphere and the mixed-layer ocean, including the positive feedback among surface wind speed, evaporation, and local SST (the WES feedback; Xie and Philander 1994; Chiang and Bitz 2005), and the stratocumulus cloud–mediated WES feedback (Hwang et al. 2017; Hsiao et al. 2022; Kim et al. 2022; Yang et al. 2023), could be responsible for the communication between the extratropical forcing and the tropical responses. On the other hand, the SST changes can also be attributed to the effect of the oceanic dynamics. For example, the oceanic subtropical cells (STCs) connect the perturbations in the deep tropics to the extratropical variations via the subduction and ventilation mechanism (Gu and Philander 1997), constraining the equatorial zonal SST gradient in both observations and simulations in global climate models (GCMs; Burls and Fedorov 2014; Fedorov et al. 2015). For the equilibrium state, studies using fully coupled models all show an equatorial peak of anomalous SST, which is distinct from the interhemispheric pattern in the slab ocean models (SOMs; Kang et al. 2020; Tomas et al. 2016). These fully coupled studies highlight the dominant role of ocean dynamics in shaping the equilibrium SST pattern. The role of thermodynamical interaction

highlighted in slab ocean studies (e.g., Hwang et al. 2017; Hsiao et al. 2022) remains to be evaluated.

While much previous research focuses on the equilibrium response patterns and the underlying mechanisms of tropical Pacific climates to extratropical forcings, few studies explore the transient evolution. In a fully coupled experiment, Wang et al. (2018) report the warming response in the equatorial region that was established within 25 years of an abrupt Arctic sea ice loss. While the formation mechanism remains to be explored, they point to the subsurface warming below 200 m as key for the anomalous vertical advection that explains the enhanced equatorial warming. Using a Lagrangian perspective that tracks seawater's trajectory, Thomas and Fedorov (2017) report long advection time scales (close to or exceeding 60 years) for the cold anomalies in the northwestern subtropical Pacific to descend to approximately 500 m before shoaling toward the equatorial undercurrent. In contrast, the seawater in the eastern subtropics goes through a shallow pathway and has time scales close to 10 years. The mechanisms and time scales of the tropical Pacific response to extratropical energy perturbation remain unresolved questions.

Disentangling responses with different time scales is critical for resolving the formation mechanism of the equilibrium response. Moreover, we expect the responses with long time scales to persist after mitigation of anthropogenic climate change takes place. Identifying distinct characteristics for the fast and slow responses is an essential step for predicting the system's response to a time-varying radiative forcing. This missing puzzle piece motivates this study to understand the transient evolution of the tropical SST responses to extratropical forcing. By running multiple ensemble members and abruptly imposing a radiative forcing in Northern Hemisphere extratropics in a fully coupled model, we can reduce the noise arising from internal variabilities and investigate mechanisms operating with different time scales. Similar approaches have been adopted to investigate the atmospheric and oceanic mechanisms regulating the tropical Pacific under CO_2 forcing (Good et al. 2011, 2013; Heede et al. 2020; Held et al. 2010). In addition to investigating the transient evolution of the tropical Pacific SST pattern, we perform a budget analysis to investigate the formation mechanisms. Specifically, we investigate when and by what means the slow response overwhelms the fast-response pattern.

The rest of this study is organized as follows. We describe the structure of the idealized forcing in our GCM simulations and introduce our energy budget analysis in section 2. In section 3, we suggest a two-stage evolution of tropical Pacific SST response to extratropical forcings: 1) a fast response, which is primarily shaped by thermodynamic air–sea interaction, where equatorial oceanic dynamics enhances and alters the pattern; and 2) a slow response that can be attributed to the change in the shallow oceanic meridional overturning circulations. We will show that the initial equatorial cooling associated with the fast response delays the emergence of the slow warming; meanwhile, the wind and temperature anomalies of the fast response set up the oceanic circulation changes of the slow responses. Therefore, investigating the transient evolution is essential for understanding the mechanisms and time scales of the equilibrium

responses. Finally, section 4 summarizes the findings, and we discuss their implications in section 5.

2. Method

a. Model setup

This study uses the NCAR Community Earth System Model (CESM), version 1.2.0 (Hurrell et al. 2013). The atmospheric model is the Community Atmospheric Model, version 5 (CAM5), with a 1.9° latitude × 2.5° longitude horizontal resolution and 30 levels. The Parallel Ocean Program, version 2 (POP2), is adopted for the oceanic component. The POP2 model uses the "gx1v6" displaced pole grid, which has a resolution of ~1° near the equator.

To isolate the pattern formation mechanisms without oceanic dynamics, we also use a SOM configuration of CESM 1.2.0. In the SOM, the dynamical ocean model is replaced by a motionless slab ocean, with fixed climatological mixed-layer depth and seasonally varying oceanic heat convergence to reproduce the mean climate simulated in the dynamical ocean model.

b. Experimental design

Following Kang et al. (2019), the experiments in this study are perturbed by either increasing or reducing the incoming solar flux at the top of the atmosphere (TOA) in the extratropics between 45° and 65°N as heating or cooling forcing. The forcing structure is shown in Fig. 1a. The forcing was originally designed to investigate the influence of extratropical cloud biases on tropical precipitation (Kang et al. 2019), and the effective forcing at the surface is approximately 0.8 PW in the annual mean. However, the simulation results can be generalized to help understand any persistent energy perturbation in the extratropics, including the anthropogenic scattering aerosols and the associated shortwave cloud changes in global warming scenarios.

To isolate the forced responses from the system's internal variability, all heating and cooling cases using the SOM and dynamical ocean models (DOMs) contain a set of 30 ensemble members. The ensemble members are branched from 30 consecutive January conditions from the corresponding control SOM and DOM simulations under preindustrial forcing. We have additionally performed a set of forced simulations that start with September, and the spatial patterns of the fast and slow responses do not depend on starting dates (not shown). The lengths of the control simulations are 50 years for SOM and 180 years for DOM, and the forced experiments are run for 6 years for SOM and 30 years for DOM. In addition, one of the 30 SOM ensembles is further integrated for 50 years to investigate the equilibrium response in the SOM.

c. The linear response

The linear component of the response is defined as the difference between the individual responses in the heating and the cooling cases, scaled by a factor of 1/2:

$$R = \frac{R_H - R_C}{2}, \tag{2.1}$$

where R is defined as the "response," and R_H and R_C denote the corresponding responses in the heating and the cooling
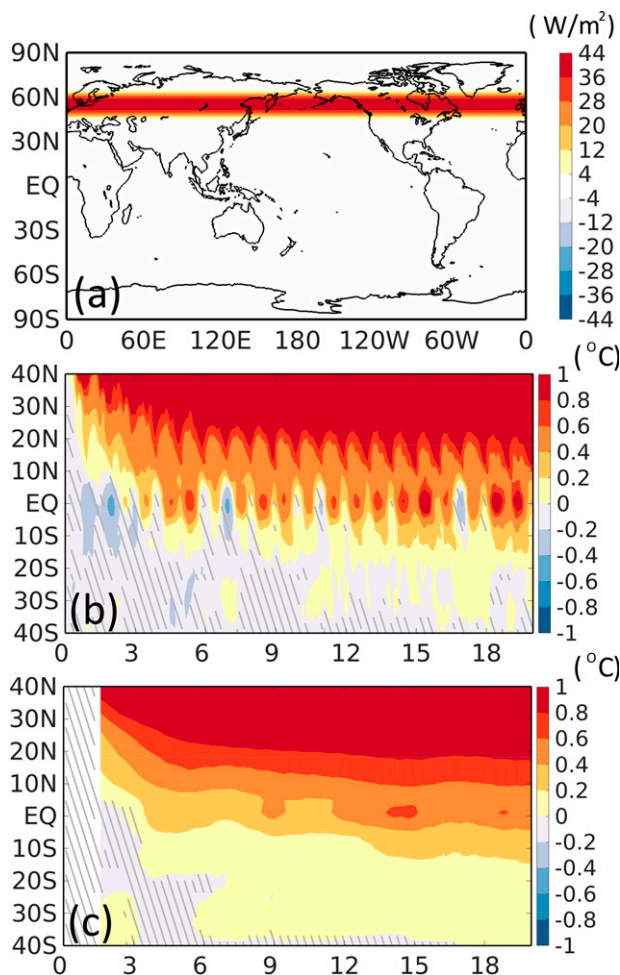
FIG. 1. The forcing profile and time series of zonally averaged SST responses. (a) The geographical distribution of incoming solar flux perturbations (W m^{-2}) in the heating case. (b) Monthly and (c) 3-yr running-averaged, anomalous zonal-averaged SST in the Pacific basin (between 160°E and 90°W). Hatching indicates where the signals are not statistically significant at the 95% confidence interval.

cases, respectively. Fig. A1 demonstrates the nonlinear surface temperature responses $[(R_H + R_C)/2]$, which are small and not statistically significant in the tropics. In the rest of the paper, only the linear components of the responses are discussed.

d. Energy budget analysis

We use an energy budget decomposition to diagnose the causes of the ocean temperature response. Considering an arbitrary finite-volume box in the ocean, one can write the energy budget in flux form, as follows:

$$C\frac{\partial T'}{\partial t} = \text{SHF}' - (\nabla UT + \nabla VT + \nabla WT)', \qquad (2.2)$$

where C represents the heat capacity of the column of water, T represents the column-averaged temperature, SHF is the surface flux into the box, $(\nabla UT + \nabla VT + \nabla WT)$ represents

the heat divergences from zonal, meridional, and vertical directions, and the prime represents the response to the forcing. Integrating both sides of Eq. (2.2) and rearranging it yields

$$\int \frac{\partial T'}{\partial t} dt = \frac{1}{C} \int [\text{SHF}' - (\nabla UT + \nabla VT + \nabla WT)'] dt. \qquad (2.3)$$

We rename each term in Eq. (2.3) as the following:

$$\text{tendency} = d\text{SHF} + d\text{UT} + d\text{VT} + d\text{WT} \qquad (2.4)$$

We can further decompose the $\nabla VT(d\text{VT})$ term, which we find to typically be the dominant term balancing the temperature tendency, into contributions of anomalous temperature, velocity, and a nonlinear term:

$$-\nabla(VT)' = -(\nabla VT') - (\nabla V'T) - (\nabla V'T') + \text{residual} \qquad (2.5)$$

and rename each term in Eq. (2.5) to be

$$d\text{VT} = \text{VdT} + \text{TdV} + \text{dVdT} + \text{Vres}. \qquad (2.6)$$

With Eqs. (2.4) and (2.6), we can quantitatively measure each component's contribution to ocean temperature responses.

3. Results

a. Tropical SST evolution

We first demonstrate the transient evolution of the tropical Pacific SST responses to extratropical thermal forcings. As shown in Figs. 1b, 1c and 2, the evolution of equatorial Pacific SST exhibits two stages: 1) a fast response, which, despite the imposed heating, is characterized by the anomalously cooled SST during the first 3 years, particularly in boreal winter; and 2) a slow response, which features gradually enhanced warmed SSTs after the third year.

Figures 3a and 3b demonstrate the distinct spatial characteristics of the two stages. The fast response shows a hemispherically asymmetric pattern, with warmed SST and weakening trades in the Northern Hemisphere (NH) and cooled SST and strengthening trades in the Southern Hemisphere (SH). Slight cooling is exhibited at the equator, accompanied by anomalous equatorial easterlies. The interhemispheric SST gradient and the cross-equatorial wind are intensified in the slow response; however, an enhanced warming in the eastern equatorial Pacific emerges and the easterlies on the equator weaken.

As a comparison, Figs. 3c and 3d present the responses in the SOM. The fast response in the DOM and that in the SOM share some resemblances (cf. Figs. 3a,c), as pointed out in previous studies investigating responses to Arctic sea ice loss (e.g., Wang et al. 2018), indicating the similar mechanisms shaping the SST structure between the two cases in the fast response. A close comparison in the equatorial region reveals a cooling peak at the central equatorial region only in the DOM (Fig. 3e), which we will later discuss in section 3b. As time evolves, ocean dynamics leads to an enhanced warming in the equatorial eastern Pacific in the DOM and completely flips the anomalous equatorial zonal gradient (cf. Figs. 3e,f); while in the SOM, though intensified, the zonal structure of
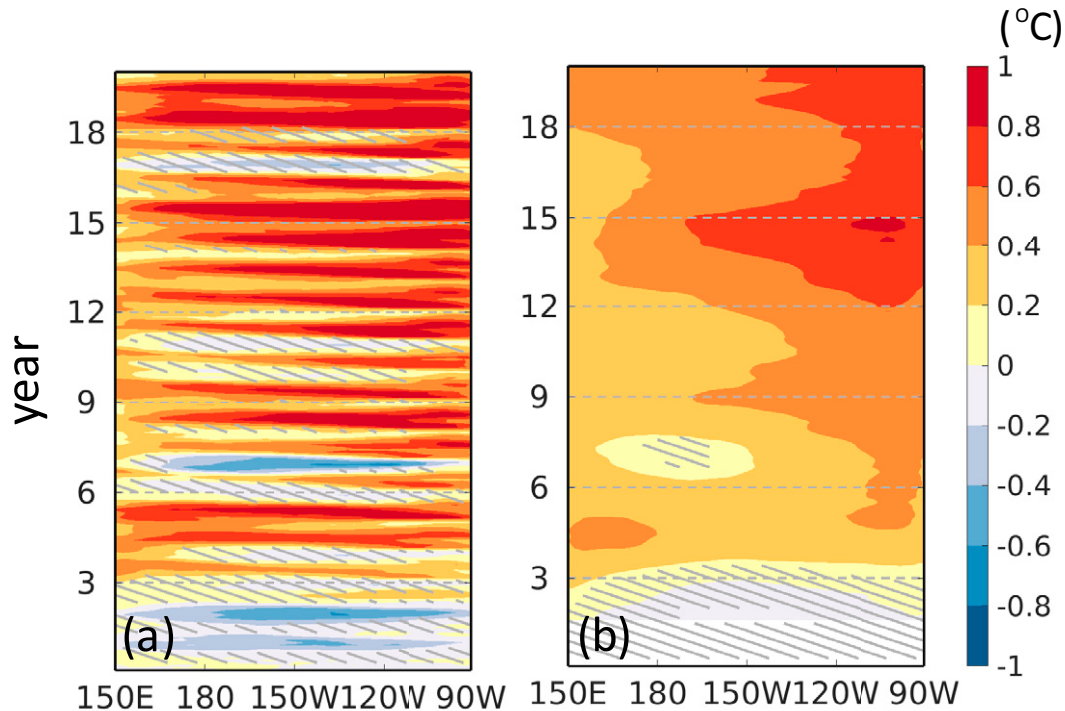
FIG. 2. Time series of equatorial Pacific SST responses. (a) Monthly and (b) 3-yr running-averaged, anomalous equatorial Pacific (averaged between 2°S and 2°N) SST (°C). Hatching indicates where the signals are not statistically significant at the 95% confidence interval.

the anomalous SST along the equator remains largely the same.

For Figs. 3a and 3b and the rest of the paper, we define the average response in years 1–3 as the fast response and the average response in years 11–20 as the slow response. Since the transition takes place gradually and the slow response continues to amplify until the end of the simulations (year 20), the start time of year 11 for the slow response is a subjective choice. Although the formation mechanisms presented in the following two sections are not sensitive to the periods chosen, we utilize 30 ensemble members to obtain a more precise estimate of the start time of the slow response. The time scale for the anomalous warming in the eastern equatorial Pacific becomes statistically significant around year 4, sooner than the 20 years reported by Wang et al. (2018), of which forcing is weaker and in a higher latitude, indicating a response of smaller magnitude (Yoshimori et al. 2017). The interannual time scale reported here and the decadal time scales reported by Wang et al. (2018) are much shorter than the time scale assumed by some previous studies focusing on the equilibrium response (Cvijanovic and Chiang 2013; Kang et al. 2020).

Note that the dominant formation mechanisms in our simulations should be distinguished from those discussed in most of the global warming literature, as greenhouse forcing is effectively globally uniform. Since the imposed heating is outside the tropics, the mechanism of the fast response differs from the dynamical thermostat mechanism discussed in CO_2 experiments, where the cooling is caused by radiative forcing within the tropics (Clement et al. 1996; Heede et al. 2020). In sections 3b and 3c, we will discuss the formation mechanisms of the two stages in detail. The possibility of using these experiments to understand tropical SST pattern evolutions under anthropogenic climate change will be discussed in section 5.

b. The formation mechanisms for the fast response

Figure 4 exhibits the zonal structures of the circulation and ocean temperature responses in the equatorial Pacific region. Consistent with the SST cooling in the equatorial central Pacific, the equatorial easterlies and the Walker circulation have strengthened slightly and shifted westward (Fig. 4a). The corresponding equatorial undercurrent has strengthened (see contours in Fig. 4e). The anomalous cooling responses appear in the upper ocean (above 50 m; Fig. 4e). It maximizes in the central Pacific and seems to be disconnected from the upwelling in the eastern Pacific or tilting thermocline.

To investigate the establishment of the equatorial cooling, we examine the first-year SST and surface wind evolution in Figs. 5a–d. The imposed extratropical radiative forcing tends to warm local SSTs in boreal spring in the NH. The warmed SST propagates toward the tropics in boreal summer (Figs. 5a,b), while the accompanied reduced trades along the northeast–southwest pathway indicate the role of the WES feedback in the equatorward propagation of anomalous SSTs in the NH. Meanwhile, the interhemispheric temperature gradient leads to the development of an anomalous, counterclockwise, cross-equatorial atmospheric meridional overturning circulation (Fig. 6a). The
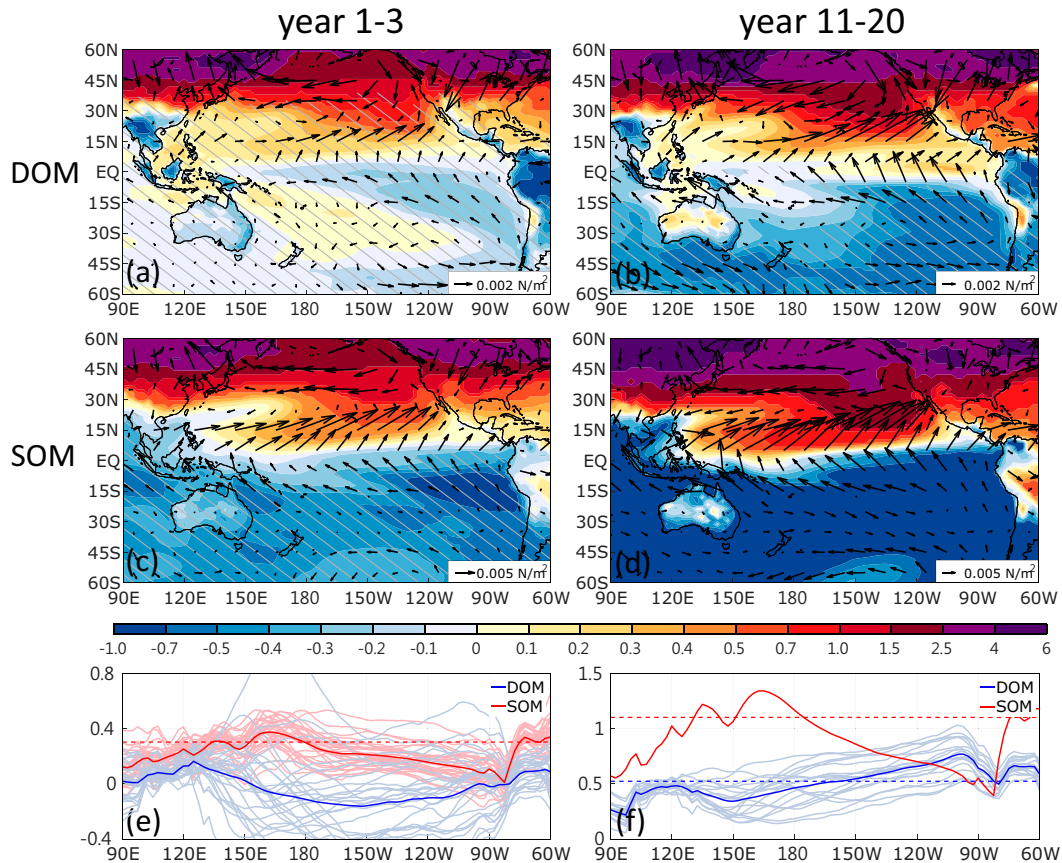
FIG. 3. Two-stage response in the tropical Pacific region. Anomalous SST relative to the tropical Pacific (20°S–20°N, 160°E–90°W) mean (°C; shading) and surface wind stress (vectors) in the period of (a) fast responses (years 1–3) and (b) slow response (years 11–20). (c),(d) As in (a),(b), but for the first 3 years and the equilibrium responses in the SOM, respectively. Anomalous equatorial Pacific (5°S–5°N) SST profile in the DOM (blue) and SOM (red) experiments for (e) fast response (years 1–3) and (f) slow response (years 11–20). Hatching in (a)–(d) indicates where the signals are not statistically significant at the 95% confidence interval. Note that regions with blue shading do not necessarily cool but do warm less than the tropical mean. The horizontal dashed lines in (e) and (f) indicate the value of the averaged SST response in the tropical Pacific region in the DOM (blue) and the SOM (red) simulations, respectively.

anomalous southerly winds in the lower branch of the anomalous overturning circulation strengthen the trades in the SH and cools local SSTs via the WES feedback. The positive feedback mechanism between low clouds, SST, and shortwave radiative fluxes further amplifies the SST anomalies in the southeastern Pacific region (Hsiao et al. 2022; Hwang et al. 2017; Kim et al. 2022). The enhanced cooling propagates equatorward via the WES feedback and reaches the central and eastern equatorial region in boreal summer and fall (Figs. 5c,d), cooling the equatorial SST during this period. Furthermore, the similarity of SST and wind responses between the DOM and SOM simulations supports the idea that the aforementioned air–sea thermodynamic interaction processes are responsible for the extratropical–tropical teleconnection and the initiation of the anomalous equatorial SST response (cf. Figs. 5a—h).

While the overall pattern and the formation mechanisms look similar in the SOM and DOM, the anomalous cooling in the equatorial region only occurs in the DOM simulation (see

Fig. 3e for the anomalous cooling in the first 3 years). To understand how ocean dynamics leads to the equatorial cooling, we perform an energy budget analysis in the upper layer of the equatorial Pacific region (2°S–2°N, 160°E–90°W, 0–50 m). As demonstrated in Fig. 7, the anomalous cooling can mainly be attributed to the anomalous meridional heat divergence (dVT), which is largely due to changes in velocity (TdV). Equatorial Ekman transport may hold the keys to the anomalous meridional heat divergence: the establishment of the anomalous equatorial easterlies initiated by the increased zonal SST gradient (Figs. 4c and 6c) drives divergent Ekman currents on the equator. The poleward Ekman transport on either hemisphere carries water and heat away from the equator, leading to local heat loss, and, hence, cools equatorial SSTs. Such mass and heat divergence in the upper layer are supported by the shallow meridional overturning circulation strengthening near the surface on both sides of the equator (Fig. 6e). Since the anomalous easterlies peak at about
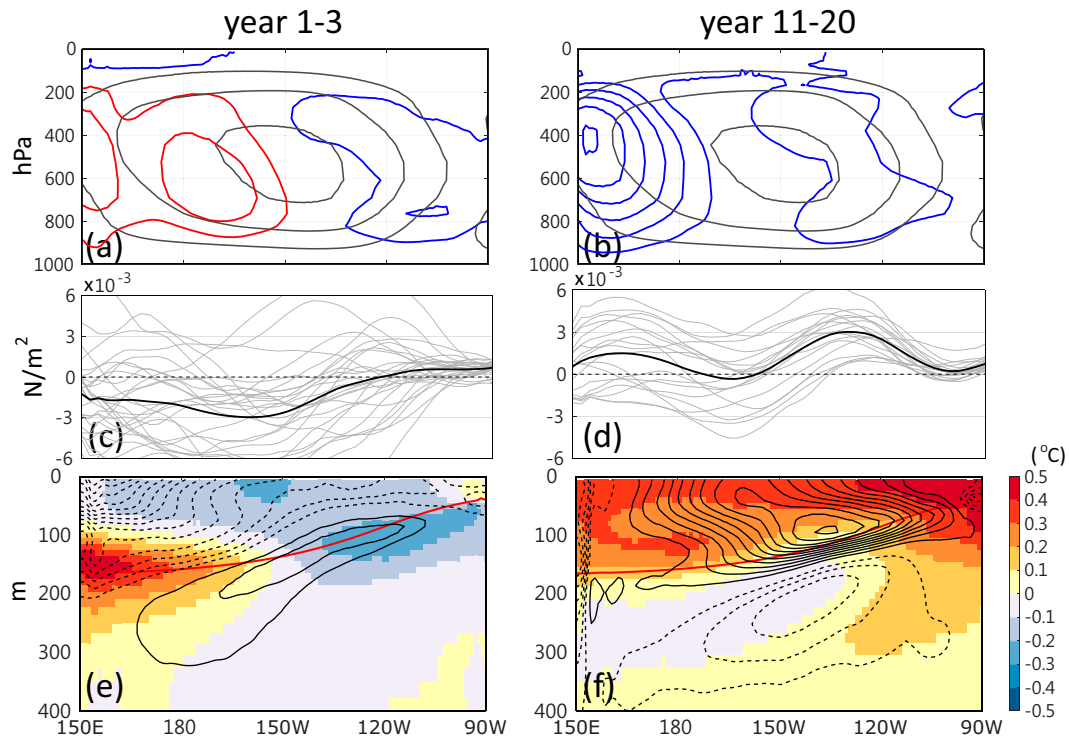
FIG. 4. Equatorial response. (a) Climatological Walker circulation [black contours with contour interval (CI) = 2 × 10⁸ kg s⁻¹; zero contour omitted and negative dashed] and the anomalies [CI = 2 × 10⁷ kg s⁻¹; red for positive (clockwise), blue for negative, and zero contour omitted]. (c) Anomalous equatorial (averaged between 2°S and 2°N) zonal stress (N m⁻²; black contoured for ensemble mean and gray for each ensemble). (e) Anomalous equatorial ocean temperature (shaded) and zonal velocity (black contoured with CI = 0.2 cm s⁻¹; zero contour omitted and negative dashed) in the period of the fast response. The climatological 20°C isotherm is superimposed as a red contour. (b),(d),(f) As in (a), (c), and (e), respectively, but for the slow response.

150°W, the corresponding Ekman divergence shifts the SST cooling response toward the central Pacific region in the DOM simulation (cf. the zonal structure of the anomalous SSTs in the SOM and the DOM in Fig. 3e).

On the other hand, the contribution from vertical advection is positive. This unexpected warming contribution may be due to surface cooling weakening upper-ocean stratification, which

may have a stronger effect on the near-surface fast response than the strengthened upwelling reported in recent studies (Kang et al. 2020; Heede et al. 2020). We focus on the mixed-layer budget based on the maximum cooling anomaly in the upper 50 m of the central Pacific (Fig. 4e). Although the contribution from vertical advection is sensitive to the depth and extent chosen, it is not the most significant factor in years 1–3.
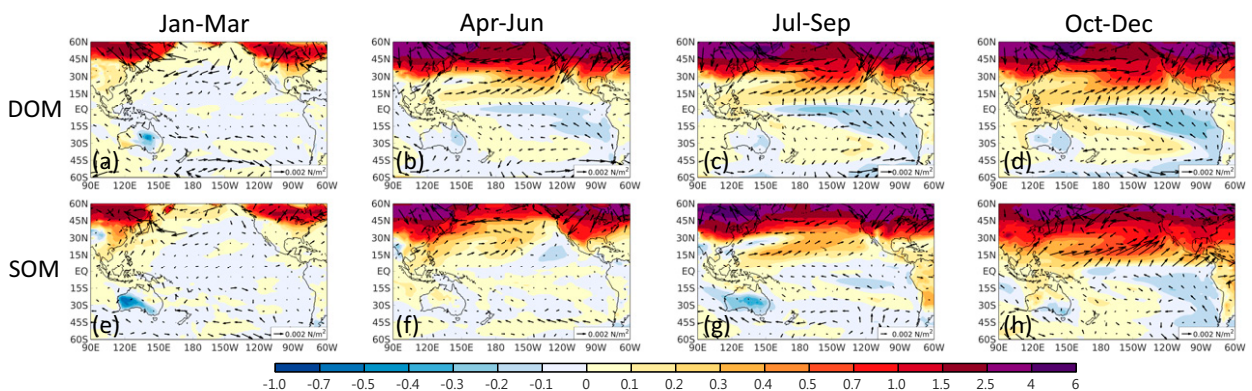

FIG. 5. Seasonal cycle during the first year. Anomalous SST (shading) and surface wind stress (vectors) during (a) January–March, (b) April–June, (c) July–September, and (d) October–December in the first year. (e)–(h) As in (a)–(d), but for the SOM.
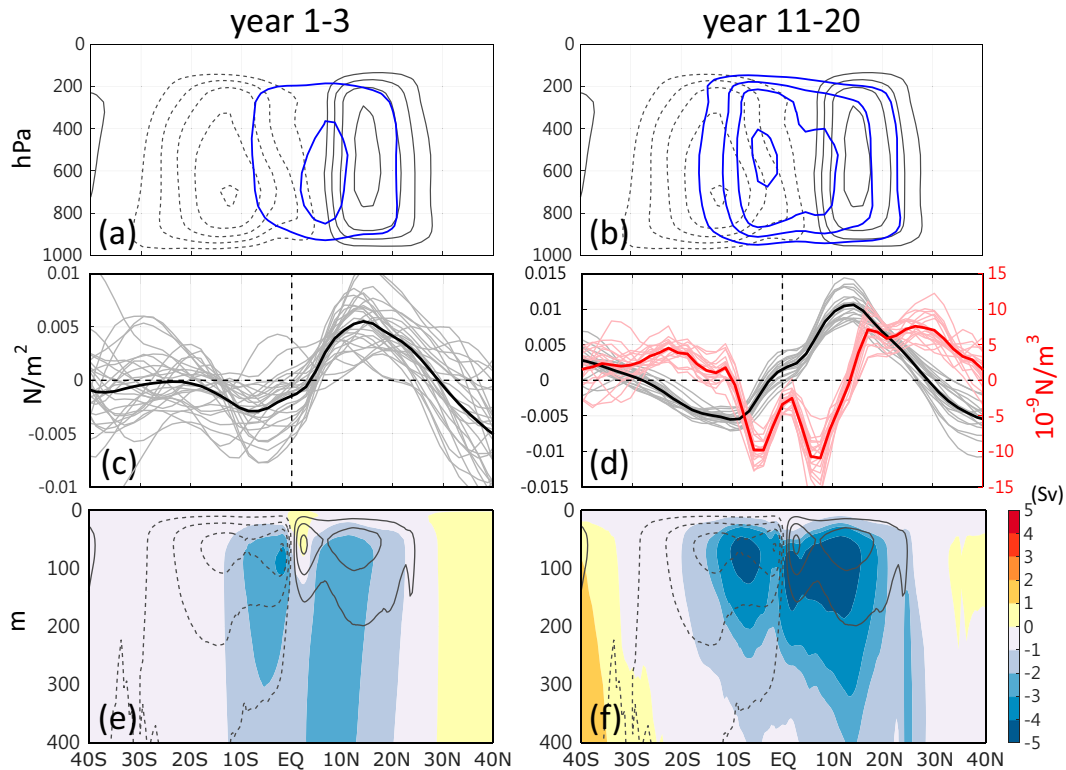
FIG. 6. Anomalous meridional overturning circulation (MOC) in fast responses. (a) Climatological atmospheric meridional mass streamfunction (black contours; CI = 2×10^8 kg s^{-1}; zero contour omitted and negative dashed) and the anomalies (CI = 1×10^8 kg s^{-1}; blue for negative, and zero contour omitted). (c) Anomalous surface zonal wind stress in the Pacific region (averaged between 160°E and 90°W). Light lines are for ensemble members, and dark for the ensemble mean. (e) Climatological oceanic MOC [black contours; CI = 10 Sv (1 Sv $\equiv 10^6$ m^3 s^{-1}); zero contour omitted and negative dashed] and the anomalies (shaded) in the Pacific region during the period of the fast response. (b),(d),(f) As is (a), (c), and (e), respectively, but for slow response. In (d), the anomalous wind-stress curl (10^{-9} N m^{-3}) in the Pacific region is superimposed as red lines.

In summary, within a few months, the air–sea coupling feedback mechanisms communicate the imposed warming from the North Pacific toward the equatorial western Pacific. Meanwhile, the cooled local SST due to the strengthened trades in the SH subtropics propagates toward the eastern and central Pacific, leading to the equatorial cooling response, despite the strong heating imposed in the northern extratropics. The intensified equatorial SST gradient and enhanced easterlies along the equator give rise to the anomalous, wind-driven, poleward Ekman transport, amplifying the cooling in the central equatorial Pacific (Figs. 3a,e).

c. The formation mechanisms for the slow response

Around the fourth year, the cooling maximum in the equatorial central Pacific diminishes and then is gradually replaced by the anomalous warming that peaks in the equatorial eastern Pacific and persists toward the end of our simulation (Figs. 2 and 3b). The Walker circulation (Fig. 4b), the equatorial easterlies (Fig. 4d), and the equatorial undercurrent (contours in Fig. 4f) experience weakening during this period, consistent with the warmed upper-ocean temperature (shading in Fig. 4f).

Following the analysis for the fast response (section 3b), we perform the upper layer energy budget (above 50 m) to investigate the warmed equatorial SST during this period. Figure 8a displays the heat budget during years 1–10 and years 11–20, accounting for the development and maintenance periods of the anomalous warming, respectively. In both periods, the vertical advection (dWT) is positive, indicating either the warmer subsurface water or the reduced upwelling could contribute to surface warming (Fig. 4f). The concept that the equatorial SST warming is originated from below is consistent with some previous studies, which indicate the dominance of the upwelling of anomalously warm subsurface water leading to warming in the equatorial eastern Pacific (England et al. 2020; Kang et al. 2020; Wang et al. 2018).

However, the warming is not confined in the upper 50 m of ocean; rather, the entire oceanic layer above the thermocline warms significantly (Fig. 4f). What causes the anomalous warming in the subsurface? To answer this question and to further examine the root cause of the positive contribution of the dWT term, we extend our energy budget analysis to 200 m (Fig. 8b). We first focus on the developing period (years 1–10), which reveals that the anomalously positive meridional dVT is
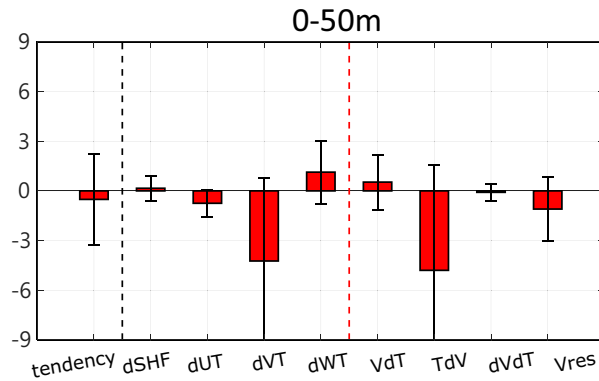
0-50m

FIG. 7. The upper-layer heat budget for fast response. Temporally integrated, anomalous heat convergence (°C) of the upper layer in the equatorial Pacific region (2°S–2°N, 160°E–90°W, surface to 50 m) during the period of the fast response. See Eqs. (2.4) and (2.6) for the definition of each term and the derivation of the decomposition. The error bars mark the one standard deviation departure from the ensemble mean of each variable.

the most prominent term. A further decomposition shows its positive contribution arises from the TdV, and its positive contribution persists in the maintaining period (years 11–20). In the following two paragraphs, we introduce the physical mechanisms leading to the positive TdV, which we interpret as the key driver leading to the equatorial warming within a decade. We also explain the relevance of other budget terms throughout the two periods.

First, we attribute the positive contribution of the TdV term to changes in the STC. Note that the process responsible for the TdV differs from the Ekman divergence discussed in section 3b, since the TdV considered here is deeper than the Ekman layer. Figure 6f illustrates the STC changes. An anomalous counterclockwise circulation develops, weakening the northern STC while strengthening the southern STC. The anomalous STC is caused by the anomalous surface wind and air–sea interactions associated with the cross-equatorial Hadley cell. According to Luongo et al. (2022, 2023), the hemispherically asymmetric surface wind stress drives shallow

STC anomalies while the joint cloud–WES feedback under the northeast Pacific low cloud deck drives a deeper buoyancy-driven cell in the NH. The slowdown of the northern STC results in less heat carried poleward, and the intensification of the southern STC acts to transport more energy away from the equator. The reduced poleward energy transport of the deeper and stronger anomalous northern cell overwhelms the increased transport of the southern cell (see the blue shading in Fig. 6f). Consequently, excessive heat accumulates in the subsurface equatorial region, eventually upwelling in the eastern equatorial Pacific region, forming the eastern equatorial-peaked warming SST pattern and triggering the Bjerknes positive feedback (Fig. 3b).

The contribution of the dWT term is also positive (Fig. 8b). This term can also be interpreted as a result of weakening NH STCs and warmer subsurface ocean in the equatorial region. The positive contribution from dWT is much smaller than that from dVT in the developing period, but it remains as a warming effect in the maintenance period. While the reduction of upwelling and weakening of STC continue to enhance the warming throughout the simulation, their effects are compensated by the term VdT in the maintenance period (years 11–20). The negative contribution of VdT can be understood as the climatological meridional advection transporting anomalously warmed water away from the equator. This explains why the anomalous meridional dVT is the most prominent term contributing positively, while it turns into a damping term in the maintenance period.

To summarize, as a response to the imposed extratropical radiative forcing, the strong weakening of the northern STC outweighs the slight strengthening of the southern STC, introducing a warm anomaly at the Pacific equatorial subsurface, which is then upwelled in the eastern equatorial region, shaping the eastern equatorial-enhanced SST warming on interannual to decadal time scales.

4. Summary and discussion

The present study investigates the transient evolution of the tropical SST pattern response to a heating imposed in the northern extratropics. While the interhemispheric SST gradient
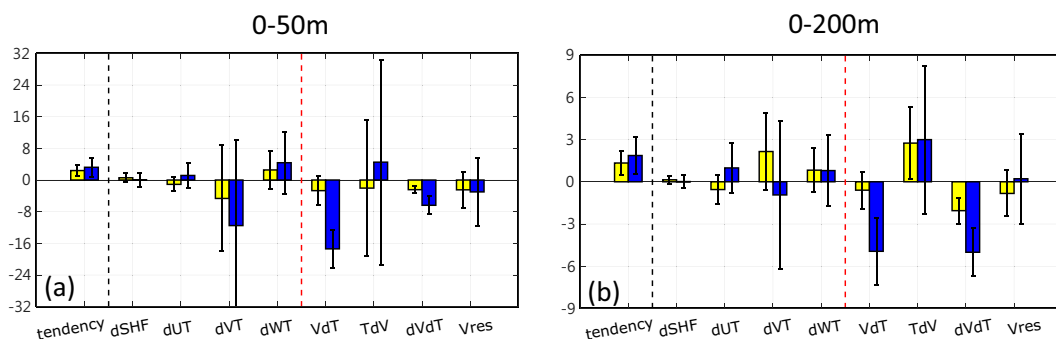

FIG. 8. Upper-layer heat budget. Temporally integrated, anomalous heat convergence (°C) of the upper layer in equatorial Pacific region (2°S–2°N, 160°E–90°W, surface to 50 m) during years 1–10 (yellow) and 11–20 (blue). See Eqs. (2.4) and (2.6) for the definition of each term and the derivation of the decomposition. The error bars mark the one standard deviation departure from the ensemble mean of each variable. (b) As in (a), but for surface to 200 m.
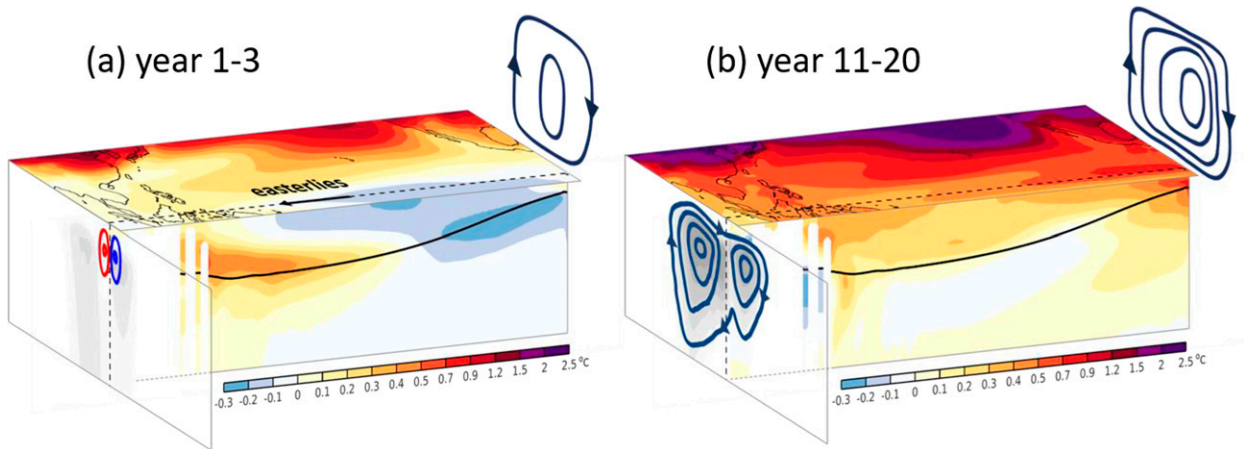
FIG. 9. Schematic diagrams of the two-stage response. (a),(b) The Hadley cell adjustments are shown on the right, while the meridional overturning circulation (STC) adjustments are shown by shading on the left. Color fill is SST and subsurface temperature response, as in Figs. 3 and 4. In (a), the hemispherically symmetric parts of the anomalous meridional overturning circulations are superimposed as contours (CI = 1.5 Sv; positive in red and negative in blue). In (b) the contours mark the total meridional overturning circulation responses (same as shading). The black contours in the vertical panels refer to the climatological 20°C isothermal line.

continues to amplify throughout the 20-yr simulations, there is a two-stage response of the equatorial zonal structure, as summarized in Fig. 9: 1) During the first 3 years, there is a slight SST cooling in the equatorial central Pacific. A series of air–sea interactions associated with the anomalous cross-equatorial Hadley cell give rise to the cooling response, while the anomalous poleward Ekman transport driven by the strengthened equatorial easterlies further amplify it. 2) The cooling is replaced by the eastern equatorial-enhanced SST warming within a decade, which continues to amplify toward the end of the simulation. We suggest that the STC slowdown in the NH leads to anomalous warming above the thermocline in the equatorial region. The warm water upwells from the east and triggers the Bjerknes feedback. In a sense, the interhemispherically asymmetric surface wind and the associated air–sea interactions in the fast response drive the anomalous STC and set the stage for the slow response. Meanwhile, the equatorial cooling in the fast response delays the time when the slow response emerges.

In the following, we connect the mechanisms summarized above to the existing literature.

a. The fast response, the ITCZ-blocking effect, and Ekman transport

The notion that the overall tropical SST pattern response and the formation processes in the fast response can be captured and explained by the SOM setting is consistent with the simulated results in Wang et al. (2018) and the hypotheses proposed by Kang et al. (2020). The fast response can be interpreted as the anomalous tropical Pacific SST pattern associated with an anomalous cross-equatorial Hadley cell. The joint cloud–WES feedback in the SH subtropics extends toward the central and eastern Pacific, whereas the warm SST anomalies from the NH midlatitudes fail to reach the same region but do propagate toward the western equatorial Pacific region. The ITCZ-blocking theory could explain why the SST response in the equatorial region exhibits an opposite sign to

the imposed forcing in the northern extratropics (Hsiao et al. 2022; Kang et al. 2020; Zhang et al. 2014). The equatorward propagation of SST anomalies cannot penetrate the location of the climatological ITCZ, where the mean meridional winds change direction, since the mean meridional winds are responsible for the WES feedback.

Besides the ITCZ blocking and the common air–sea interactions in the SOM and the DOM, the present study additionally highlights the critical roles of ocean dynamics in altering the equatorial zonal SST structure in the DOM. The poleward Ekman transport driven by anomalous easterlies further amplifies the cooling originated from the SH subtropics and shifts the maximum cooling from the eastern toward the central equatorial Pacific (Figs. 3e and 9a). The equatorial zonal SST gradient and the Walker cell responses are distinct in the SOM and the DOM in the first 3 years.

b. The slow response and the role of STC changes

The slowly emerging, enhanced equatorial SST warming pattern, according to our 50-m budget analysis, is attributed to the upwelling of anomalously warmed subsurface water. The notion that the enhanced equatorial response originates from the subsurface is consistent with previous studies (England et al. 2020; Kang et al. 2020; Wang et al. 2018). These studies consider the subsurface warming to originate from the ventilation and subduction mechanism, where SST anomalies are advected from midlatitudes toward the tropics by the lower branches of the climatological STCs (Deser et al. 1996; Gu and Philander 1997; Sasaki et al. 2010).

Our transient budget analyses reveal that processes contributing positively in the equilibrium responses may differ from those that are responsible for initiating the pattern formation. For example, in contrast to previous studies that focus on equilibrium responses, our results show that the temperature anomalies advected by climatological flow (VdT in Fig. 8b) contribute negatively to the warming during years 11–20.

Instead, we attribute the warming to the weakening of the northern STC (TdV), which develops within the first few years (Fig. 6e). Accompanied by the accumulation of the anomalous heat divergence at the equator, the anomalous northern STC persists in the slow response, leading to the pronounced warming in the upper ocean observed after the first decade. The decadal time scale of the oceanic circulation adjustment is much faster than that of the subduction and ventilation mechanism, which is considered to be a multidecadal process (Thomas and Fedorov 2017). Despite the significant dominance of TdV in our budget (Fig. 8b), we should not exclude the effect of VdT on the equatorial Pacific SST. Although it appears to be a minor factor in our experiments, if we were to extend our simulations to a longer period, the positive contribution of VdT may take over the equatorial warming over time. The imposed heating in the extratropics should eventually find its way to warm the equatorial region through climatological advection (e.g., Kang et al. 2020). In addition, selecting meridional boundaries with a higher latitude range (e.g., 10°S–10°N) could increase the contribution of VdT in years 11–20. Further investigation is required to determine the relative roles of VdT and TdV in the equatorial Pacific SST response.

The early developing process highlights the rapid STC response to a cross-equatorial Hadley cell. We expect the equatorial ocean water to be affected through the proposed mechanism within decadal time scales. The strong coupling between the Hadley cell and STCs has been discussed in the literature in the context of the anomalous STC transporting energy across the equator and damping the ITCZ shift (Green and Marshall 2017; Hawcroft et al. 2017; Tomas et al. 2016; Kay et al. 2016; Xiang et al. 2018). Here, we focus on the equatorial SST response and highlight the effect of the hemispherically asymmetric STC changes. The hemispherically asymmetric STC changes can be interpreted via the same coupling mechanism discussed in the ITCZ-shift literature. Since the forcing is applied in the NH extratropics, the meridional SST gradient, the associated wind changes, and thus the STC response are stronger in the NH (as shown in Figs. 4d,f). The contrasting anomalous STCs in the two hemispheres are crucial to the heat convergence in the equatorial region, which eventually shapes the eastern equatorial-peaked SST pattern several years after the forcing is imposed. Meanwhile, in section 3c, we refer to the mechanisms proposed by Luongo et al. (2022), who use the same experimental setting but apply an additional wind stress–locking technique, to interpret the driver of the STC changes. Using the same experiment, Luongo et al. (2023) further confirm the critical role of buoyancy-forced STC changes in affecting the equatorial energy budget.

5. Conclusions and implication

Previous studies show that tropical zonal (east-to-west) and meridional (equator-to-pole) SST gradients vary coherently in paleo-proxy SST records and modeling simulations on multidecadal and century time scales (Fedorov et al. 2015; Burls and Fedorov 2014; Stuecker et al. 2018). The STCs and the equatorial undercurrent act as oceanic tunnels for extratropical SST anomalies to reach the surface of the equatorial eastern Pacific. Here, we emphasize the effects of the hemispherically asymmetric temperature gradient on the equatorial zonal SST gradient. In the first 3 years, the zonal SST gradient strengthens when the interhemispheric temperature gradient increases. On decadal time scales, the weakened equatorial zonal SST gradient is consistent with what would have been expected from the weakened equator-to-pole SST gradient. We additionally highlight the contribution from the hemispherically asymmetric, forcing-induced STC changes, which operate on a time scale much shorter than the ventilation and may be detectable in the observational records or near-future climate change projections.

The two-stage response revealed in the present study demonstrates the complexity of interhemispherically asymmetric energy perturbations on tropical Pacific SST responses. Improving our understanding of the extratropical to tropical teleconnection would enhance our confidence in the future projections of the tropical Pacific region under anthropogenic climate change. We discuss some related open questions below.

a. Linkages with the GHG-forced simulations

A great number of previous studies explore the tropical Pacific SST response under global warming. The equatorial SST response and the related mechanisms and time scales discussed in these studies can be compared to those suggested in the present study.

For the fast response, our idealized forcing highlights a tropical SST formation mechanism driven by hemispherically asymmetric warming. We expect the same mechanism to operate under global warming, as a similar hemispherically asymmetric temperature and surface wind patterns exist in the CO_2 experiments (Hwang et al. 2017; Long et al. 2014). Based on our simulations, the enhanced warming in the NH extratropics contributes to the relative cooling (delayed warming) in the equatorial central Pacific in the fast response of abrupt $4xCO_2$ experiments. Heede and Fedorov (2021) take the average of the first 10 years to demonstrate the pattern of the fast response. In this study we have defined our fast response as the first 3 years, based on absolute SST. If, however, we were to plot the relative SST pattern [the anomalous warming departure from tropical mean, as in Fig. 3 in Heede and Fedorov (2021)] of the first 10 years of our experiment, a relative cooling, which is most pronounced in the southeast Pacific, persists and extends toward the equatorial central Pacific. This suggests that the joint low cloud–WES feedback and the equatorial divergent Ekman transport in our idealized experiments could play a role in explaining the fast response in abrupt $4xCO_2$ experiments. The mechanism would have a larger contribution in models with larger interhemispherically asymmetric warming (Geng et al. 2022), i.e., a larger heat uptake over the Southern Ocean or a greater Arctic amplification. The mechanism is distinct from the ocean dynamical thermostat in the context of the equatorial ocean response to a uniform surface flux perturbation (Clement et al. 1996; Seager et al. 2019; Heede and Fedorov 2021; Heede et al. 2020, 2021).

For the slow response, our idealized experiment suggests the hemispherically asymmetric STC change can lead to an accumulated warming in the equatorial subsurface, which makes its way to the surface through the upwelling in the east. The changes in the strength of STCs and the effect on SSTs emerge within the first 10 years of our simulations. Consistently, one can see a relative warming in the equatorial eastern Pacific in the anomalous SST pattern in the first 10 years of the $4xCO_2$ experiments [Fig. 3 in Heede and Fedorov (2021)]. The effect of STC changes dominating on decadal time scales is consistent with another study concerning the possible mechanisms leading to the equatorial SST warming under GHG forcing (Heede et al. 2021). They found that the change in the strength of STCs takes place much earlier than when the extratropical SST anomalies reach the equatorial region. It is not until years 350–400 that the contribution from VdT outweighs the contribution from TdV in their CO_2 forcing experiments. Compared to the effects of TdV reported in our study and by Heede et al. (2021), the effects of ventilation (VdT) may not be as relevant for the reduced equatorial zonal gradient in experiments with more realistic forcing, such as the shared socioeconomic pathways (SSPs)–type of experiments in phase 6 of the Coupled Model Intercomparison Project (CMIP6).

b. Linkages with other modeling experiments and observational records

In addition to greenhouse gases, recent studies also suggest the impacts of anthropogenic aerosols and volcanoes on the recent trend of tropical Pacific SST (Hwang et al. 2013; Takahashi and Watanabe 2016; Smith et al. 2016; Heede and Fedorov 2021). Our idealized experiments reveal that mechanisms with multiple time scales are at work in shaping the tropical Pacific SST pattern when an anomalous cross-equatorial Hadley cell adjustment takes place. Disentangling multiple time-scale responses to aerosols is essential for understanding the SST pattern evolution in the multimodel large-ensemble archive (Deser et al. 2020). The joint cloud–WES feedback and the STC adjustment highlighted in this study may contribute to discrepancies in tropical east Pacific change between models and observations (Wills et al. 2022).

c. Outlook

We have studied the response of the coupled system to energy perturbations in the high-latitude Northern Hemisphere, with a focus on the time scales and mechanisms of the ocean's dynamic response. However, it is yet to be determined how these time scales and response patterns differ across GCMs, given their varying resolutions, convection schemes, or mean-state biases. The radiative forcing in this study is concentrated in high latitudes of the Northern Hemisphere, which is relevant to global warming scenarios that show more warming in the Northern Hemisphere or to aerosol emissions that concentrate in the Northern Hemisphere extratropics. However, perturbations in the Southern Hemisphere, such as temperature anomalies caused by melting of the Antarctic ice sheet or ozone recovery, may also play a significant role in tropical climate change. Future studies need to explore whether the mechanisms demonstrated in this study can be applied to Southern Hemisphere forcings.

APPENDIX

The Nonlinear Response

Figure A1 shows the nonlinear response of SST and surface wind stress in the period of the fast responses (years 1–3) and the slow response (years 11–20).
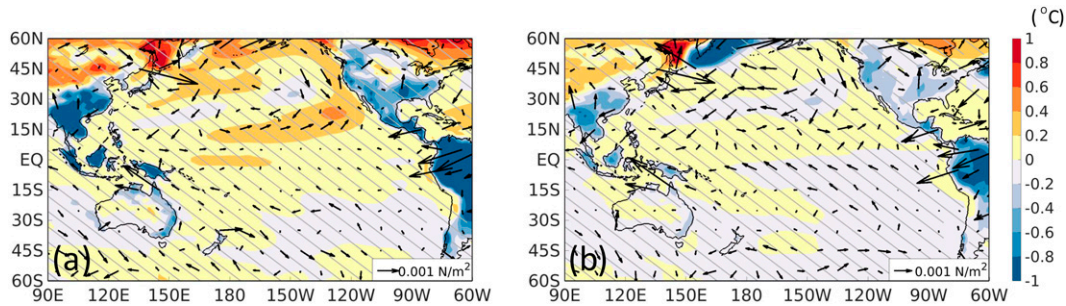
FIG. A1. The nonlinear response of SST (shading) and surface wind stress (vectors) in the period of (a) the fast responses (years 1–3) and (b) the slow response (years 11–20). Hatching indicates where the signals are not statistically significant at the 95% confidence interval.

REFERENCES

Broccoli, A. J., K. A. Dahl, and R. J. Stouffer, 2006: Response of the ITCZ to Northern Hemisphere cooling. *Geophys. Res. Lett.*, **33**, L01702, https://doi.org/10.1029/2005GL024546.

Burls, N. J., and A. V. Fedorov, 2014: What controls the mean east–west sea surface temperature gradient in the equatorial Pacific: The role of cloud albedo. *J. Climate*, **27**, 2757–2778, https://doi.org/10.1175/JCLI-D-13-00255.1.

——, L. Muir, E. M. Vincent, and A. Fedorov, 2017: Extra-tropical origin of equatorial Pacific cold bias in climate models with links to cloud albedo. *Climate Dyn.*, **49**, 2093–2113, https://doi.org/10.1007/s00382-016-3435-6.

Chiang, J. C. H., and C. M. Bitz, 2005: Influence of high latitude ice cover on the marine intertropical convergence zone. *Climate Dyn.*, **25**, 477–496, https://doi.org/10.1007/s00382-005-0040-5.

Clement, A. C., R. Seager, M. A. Cane, and S. E. Zebiak, 1996: An ocean dynamical thermostat. *J. Climate*, **9**, 2190–2196, https://doi.org/10.1175/1520-0442(1996)009<2190:AODT>2.0.CO;2.

Cvijanovic, I., and J. C. H. Chiang, 2013: Global energy budget changes to high latitude North Atlantic cooling and the tropical ITCZ response. *Climate Dyn.*, **40**, 1435–1452, https://doi.org/10.1007/s00382-012-1482-1.

Deser, C., M. A. Alexander, and M. S. Timlin, 1996: Upper-ocean thermal variations in the North Pacific during 1970–1991. *J. Climate*, **9**, 1840–1855, https://doi.org/10.1175/1520-0442(1996)009<1840:UOTVIT>2.0.CO;2.

——, R. A. Tomas, and L. Sun, 2015: The role of ocean–atmosphere coupling in the zonal-mean atmospheric response to Arctic sea ice loss. *J. Climate*, **28**, 2168–2186, https://doi.org/10.1175/JCLI-D-14-00325.1.

——, and Coauthors, 2020: Insights from Earth system model initial-condition large ensembles and future prospects. *Nat. Climate Change*, **10**, 277–286, https://doi.org/10.1038/s41558-020-0731-2.

Dong, B.-W., and R. T. Sutton, 2002: Adjustment of the coupled ocean–atmosphere system to a sudden change in the thermohaline circulation. *Geophys. Res. Lett.*, **29**, 1728, https://doi.org/10.1029/2002GL015229.

England, M. R., L. M. Polvani, L. Sun, and C. Deser, 2020: Tropical climate responses to projected Arctic and Antarctic sea-ice loss. *Nat. Geosci.*, **13**, 275–281, https://doi.org/10.1038/s41561-020-0546-9.

Fedorov, A. V., N. J. Burls, K. T. Lawrence, and L. C. Peterson, 2015: Tightly linked zonal and meridional sea surface temperature gradients over the past five million years. *Nat. Geosci.*, **8**, 975–980, https://doi.org/10.1038/ngeo2577.

Geng, Y.-F., S.-P. Xie, X.-T. Zheng, S.-M. Long, S. M. Kang, X. Lin, and Z.-H. Song, 2022: CMIP6 intermodel uncertainty in interhemispheric asymmetry of tropical climate response to greenhouse warming: Extratropical ocean effects. *J. Climate*, **35**, 4869–4882, https://doi.org/10.1175/JCLI-D-21-0541.1.

Good, P., J. M. Gregory, and J. A. Lowe, 2011: A step-response simple climate model to reconstruct and interpret AOGCM projections. *Geophys. Res. Lett.*, **38**, L01703, https://doi.org/10.1029/2010GL045208.

——, ——, ——, and T. Andrews, 2013: Abrupt CO_2 experiments as tools for predicting and understanding CMIP5 representative concentration pathway projections. *Climate Dyn.*, **40**, 1041–1053, https://doi.org/10.1007/s00382-012-1410-4.

Green, B., and J. Marshall, 2017: Coupling of trade winds with ocean circulation damps ITCZ shifts. *J. Climate*, **30**, 4395–4411, https://doi.org/10.1175/JCLI-D-16-0818.1.

Gu, D., and S. G. H. Philander, 1997: Interdecadal climate fluctuations that depend on exchanges between the tropics and extratropics. *Science*, **275**, 805–807, https://doi.org/10.1126/science.275.5301.805.

Hawcroft, M., J. M. Haywood, M. Collins, A. Jones, A. C. Jones, and G. Stephens, 2017: Southern Ocean albedo, interhemispheric energy transports and the double ITCZ: Global impacts of biases in a coupled model. *Climate Dyn.*, **48**, 2279–2295, https://doi.org/10.1007/s00382-016-3205-5.

Heede, U. K., and A. V. Fedorov, 2021: Eastern equatorial Pacific warming delayed by aerosols and thermostat response to CO_2 increase. *Nat. Climate Change*, **11**, 696–703, https://doi.org/10.1038/s41558-021-01101-x.

——, ——, and N. J. Burls, 2020: Time scales and mechanisms for the tropical Pacific response to global warming: A tug of war between the ocean thermostat and weaker Walker. *J. Climate*, **33**, 6101–6118, https://doi.org/10.1175/JCLI-D-19-0690.1.

——, ——, and ——, 2021: A stronger versus weaker Walker: Understanding model differences in fast and slow tropical Pacific responses to global warming. *Climate Dyn.*, **57**, 2505–2522, https://doi.org/10.1007/s00382-021-05818-5.

Held, I. M., M. Winton, K. Takahashi, T. Delworth, F. Zeng, and G. K. Vallis, 2010: Probing the fast and slow components of global warming by returning abruptly to preindustrial forcing. *J. Climate*, **23**, 2418–2427, https://doi.org/10.1175/2009JCLI3466.1.

Hsiao, W.-T., Y.-T. Hwang, Y.-J. Chen, and S. M. Kang, 2022: The role of clouds in shaping tropical Pacific response pattern to extratropical thermal forcing. *Geophys. Res. Lett.*, **49**, e2022GL098023, https://doi.org/10.1029/2022GL098023.

Hurrell, J. W., and Coauthors, 2013: The Community Earth System Model: A framework for collaborative research. *Bull. Amer. Meteor. Soc.*, **94**, 1339–1360, https://doi.org/10.1175/BAMS-D-12-00121.1.

Hwang, Y.-T., D. M. W. Frierson, and S. M. Kang, 2013: Anthropogenic sulfate aerosol and the southward shift of tropical precipitation in the late 20th century. *Geophys. Res. Lett.*, **40**, 2845–2850, https://doi.org/10.1002/grl.50502.

——, S.-P. Xie, C. Deser, and S. M. Kang, 2017: Connecting tropical climate change with Southern Ocean heat uptake. *Geophys. Res. Lett.*, **44**, 9449–9457, https://doi.org/10.1002/2017GL074972.

——, H.-Y. Tseng, K.-C. Li, S. M. Kang, Y.-J. Chen, and J. C. H. Chiang, 2021: Relative roles of energy and momentum fluxes in the tropical response to extratropical thermal forcing. *J. Climate*, **34**, 3771–3786, https://doi.org/10.1175/JCLI-D-20-0151.1.

Kang, S. M., I. M. Held, D. M. W. Frierson, and M. Zhao, 2008: The response of the ITCZ to extratropical thermal forcing: Idealized slab-ocean experiments with a GCM. *J. Climate*, **21**, 3521–3532, https://doi.org/10.1175/2007JCLI2146.1.

——, and Coauthors, 2019: Extratropical–Tropical Interaction Model Intercomparison Project (ETIN-MIP): Protocol and initial results. *Bull. Amer. Meteor. Soc.*, **100**, 2589–2606, https://doi.org/10.1175/BAMS-D-18-0301.1.

——, S.-P. Xie, Y. Shin, H. Kim, Y.-T. Hwang, M. F. Stuecker, B. Xiang, and M. Hawcroft, 2020: Walker circulation response to extratropical radiative forcing. *Sci. Adv.*, **6**, eabd3021, https://doi.org/10.1126/sciadv.abd3021.

Kay, J. E., C. Wall, V. Yettella, B. Medeiros, C. Hannay, P. Caldwell, and C. Bitz, 2016: Global climate impacts of fixing the Southern Ocean shortwave radiation bias in the Community Earth System Model (CESM). *J. Climate*, **29**, 4617–4636, https://doi.org/10.1175/JCLI-D-15-0358.1.

Kim, H., S. M. Kang, J. E. Kay, and S.-P. Xie, 2022: Subtropical cloud key to Southern Ocean teleconnections to the tropical Pacific. *Proc. Natl. Acad. Sci. USA*, **119**, e2200514119, https://doi.org/10.1073/pnas.2200514119.

Long, S.-M., S.-P. Xie, X.-T. Zheng, and Q. Liu, 2014: Fast and slow responses to global warming: Sea surface temperature and precipitation patterns. *J. Climate*, **27**, 285–299, https://doi.org/10.1175/JCLI-D-13-00297.1.

Luongo, M. T., S.-P. Xie, and I. Eisenman, 2022: Buoyancy forcing dominates the cross-equatorial ocean heat transport response to Northern Hemisphere extratropical cooling. *J. Climate*, **35**, 3071–3090, https://doi.org/10.1175/JCLI-D-21-0950.1.

——, ——, ——, Y.-T. Hwang, and H.-Y. Tseng, 2023: A pathway for Northern Hemisphere extratropical cooling to elicit a tropical response. *Geophys. Res. Lett.*, **50**, e2022GL100719, https://doi.org/10.1029/2022GL100719.

Sasaki, Y. N., N. Schneider, N. Maximenko, and K. Lebedev, 2010: Observational evidence for propagation of decadal spiciness anomalies in the North Pacific. *Geophys. Res. Lett.*, **37**, L07708, https://doi.org/10.1029/2010GL042716.

Seager, R., M. Cane, N. Henderson, D.-E. Lee, R. Abernathey, and H. Zhang, 2019: Strengthening tropical Pacific zonal sea surface temperature gradient consistent with rising greenhouse

gases. *Nat. Climate Change*, **9**, 517–522, https://doi.org/10.1038/s41558-019-0505-x.

Smith, D. M., and Coauthors, 2016: Role of volcanic and anthropogenic aerosols in the recent global surface warming slowdown. *Nat. Climate Change*, **6**, 936–940, https://doi.org/10.1038/nclimate3058.

Stuecker, M. F., and Coauthors, 2018: Polar amplification dominated by local forcing and feedbacks. *Nat. Climate Change*, **8**, 1076–1081, https://doi.org/10.1038/s41558-018-0339-y.

Takahashi, C., and M. Watanabe, 2016: Pacific trade winds accelerated by aerosol forcing over the past two decades. *Nat. Climate Change*, **6**, 768–772, https://doi.org/10.1038/nclimate2996.

Thomas, M. D., and A. V. Fedorov, 2017: The eastern subtropical Pacific origin of the equatorial cold bias in climate models: A Lagrangian perspective. *J. Climate*, **30**, 5885–5900, https://doi.org/10.1175/JCLI-D-16-0819.1.

Tomas, R. A., C. Deser, and L. Sun, 2016: The role of ocean heat transport in the global climate response to projected Arctic sea ice loss. *J. Climate*, **29**, 6841–6859, https://doi.org/10.1175/JCLI-D-15-0651.1.

Wang, K., C. Deser, L. Sun, and R. A. Tomas, 2018: Fast response of the tropics to an abrupt loss of Arctic sea ice via ocean dynamics. *Geophys. Res. Lett.*, **45**, 4264–4272, https://doi.org/10.1029/2018GL077325.

Wills, R. C. J., Y. Dong, C. Proistosecu, K. C. Armour, and D. S. Battisti, 2022: Systematic climate model biases in the large-scale patterns of recent sea-surface temperature and sea-level pressure change. *Geophys. Res. Lett.*, **49**, e2022GL100011, https://doi.org/10.1029/2022GL100011.

Xiang, B., M. Zhao, Y. Ming, W. Yu, and S. M. Kang, 2018: Contrasting impacts of radiative forcing in the Southern Ocean versus southern tropics on ITCZ position and energy transport in one GFDL climate model. *J. Climate*, **31**, 5609–5628, https://doi.org/10.1175/JCLI-D-17-0566.1.

Xie, S.-P., and S. G. H. Philander, 1994: A coupled ocean–atmosphere model of relevance to the ITCZ in the eastern Pacific. *Tellus*, **46A**, 340–350, https://doi.org/10.3402/tellusa.v46i4.15484.

Yang, L., S.-P. Xie, S. S. P. Shen, J.-W. Liu, and Y.-T. Hwang, 2023: Low cloud–SST feedback over the subtropical northeast Pacific and the remote effect on ENSO variability. *J. Climate*, **36**, 441–452, https://doi.org/10.1175/JCLI-D-21-0902.1.

Yoshimori, M., and A. J. Broccoli, 2008: Equilibrium response of an atmosphere–mixed layer ocean model to different radiative forcing agents: Global and zonal mean response. *J. Climate*, **21**, 4399–4423, https://doi.org/10.1175/2008JCLI2172.1.

——, A. Abe-Ouchi, and A. Laîné, 2017: The role of atmospheric heat transport and regional feedbacks in the Arctic warming at equilibrium. *Climate Dyn.*, **49**, 3457–3472, https://doi.org/10.1007/s00382-017-3523-2.

Zhang, H., C. Deser, A. Clement, and R. Tomas, 2014: Equatorial signatures of the Pacific meridional modes: Dependence on mean climate state. *Geophys. Res. Lett.*, **41**, 568–574, https://doi.org/10.1002/2013GL058842.

Zhang, R., and T. L. Delworth, 2005: Simulated tropical response to a substantial weakening of the Atlantic thermohaline circulation. *J. Climate*, **18**, 1853–1860, https://doi.org/10.1175/JCLI3460.1.